Plasma Sources
Science and
Technology

Plasma–liquid interactions on acoustically structured Faraday liquid interfaces

OPEN ACCESS
IOP Publishing
Plasma Sources Science and Technology
Plasma Sources Sci. Technol. **34** (2025) 055009 (13pp)
https://doi.org/10.1088/1361-6595/add6d5

Plasma–liquid interactions on acoustically structured Faraday liquid interfaces

R Z Walker[1,*], **S J Doyle**[2] **and J E Foster**[1]

[1] Department of Nuclear Engineering and Radiological Sciences, University of Michigan, Ann Arbor, MI, United States of America
[2] Department of Physics, School of Natural & Computing Sciences, University of Aberdeen, King's College, Aberdeen AB24 3FX, United Kingdom

E-mail: rzpinsky@umich.edu

Received 19 December 2024, revised 22 April 2025
Accepted for publication 9 May 2025
Published 23 May 2025

Abstract

Enhancing reactive species transport at the plasma–liquid interface is important for scaling of atmospheric pressure plasmas studied in the laboratory to real-world applications. It is well-known that the introduction of turbulence at any interface will enhance mixing by enhancing species uptake from the gas phase to the liquid phase by surface renewal processes, entrainment, bubbles and surface area modification. The goal of this work is to isolate surface effects associated with turbulence from the multitude of turbulent transport enhanced processes by artificially introducing surface perturbations using Faraday waves. Experiments were conducted to determine decoloration rate constants of a model contaminant (methylene blue) as a function of both discharge features (including positive and negative streamers) and hydrodynamics (Faraday surface wavelengths). The local plasma ionization wave at the interfacial structure was modeled and compared to experiments. Interestingly, it was found in experiments that plasma in contact with the water also generated capillary waves thus modifying the surface as well. Plasma ionization waves in combination with acoustic driven Faraday waves adds to the complexity of interpreting the effects of, for example, surface area increases, due to these complex coupled phenomenon. Local plasma ionization wave structure appears to be modified (increased propagation distance) when the liquid is perturbed, leading to increased contact of the liquid water surface with reactive species. Along with interfacial surface area growth, nonlinear convective transport is also increased with perturbations, leading to the general realization that acoustic perturbations can improve transport and thus decoloration of the model contaminant dye.

Supplementary material for this article is available online

Keywords: plasma, Faraday wave, interface, surface area

* Author to whom any correspondence should be addressed.

1. Introduction

Often neglected in studies involving the interaction of plasma with liquid water is the time dependent changes in the surface morphology of the water itself. In fact Lindsay, Lai and others have shown experimentally how plasma-induced mixing effects at the interface can affect gas phase uptake into the liquid [1–3]. The surface ultimately determines the collection area for transport. If it is in motion, it can also affect diffusion processes. Wave effects and localized heating can further influence transport across the interface and induce convection which enhances mixing [2, 4]. Flowing water surfaces often feature turbulent morphologies which greatly influence transport via mixing through convective motion, enhanced surface area, entrainment and large effective diffusion coefficients [5, 6]. Turbulent surfaces therefore likely play a key role in transport and thus provides insight into processes prevailing at the plasma–liquid interface. Indeed, previous work has shown that turbulent surfaces in the presence of plasma can give rise to enhance degradation rates of model contaminants in water [7].

The study of both hydrodynamic and plasma processes occurring simultaneously with turbulent liquids is challenging. The effect of turbulence on the physical mechanisms leading to decomposition of contaminants is multi-faceted. The interface is constantly moving stochastically, making it difficult to form conclusions at the spatio-temporal scales of interest (even when modeled). In addition, hydrodynamic bulk forces as well as surface morphological changes both play a role in the transport of reactive species to the interface (and contaminants to the interface). Given that transport of reactive species across the gas–liquid interface is a key driver in plasma water treatment, it naturally follows that manipulating the interface can alter the effectiveness of this treatment. The goal of this work is to investigate time-dependent, regular oscillations on the surface. This approach couples time-dependent variations in surface with plasma morphological effects. Thus, this work aims to elucidate the impact of interfacial structural changes at the plasma–liquid interface in a controlled manner via Faraday waves. Here, insight is gained on the fate of gas phase plasma produced products which are subject to diffusive, convective, and discharge properties along the interfacial region. Both amplitudes of surface oscillations and characteristic length scale of the perturbation are known and can be controlled acoustically.

The observation of Faraday waves dates back to 1831 with Michael Faraday's first publication on the subject [8]. The perturbations are actually not traveling waves but rather a localized standing wave. Since then, many researchers have focused on the generation and application of these surface perturbations. Essentially, the Faraday wave instability is a parametric oscillator that can be excited by some forcing mechanism, such as acoustic excitation [9, 10]. Equation (1) gives the instability for a given frequency. The addition of an electric field can also influence the wave structure (as opposed to or in conjunction with, for example, an acoustic driver). Faraday waves can be subdivided into two categories: gravitational waves or capillary waves. At a critical transition wavelength of around 2.7 mm, surface tension forces dominate and gravity can essentially be neglected, giving rise to capillary waves.

$$\omega^2 = \left(gk + \frac{\gamma k^3}{\rho}\right) \tanh\left(kh_0\right). \tag{1}$$

In this equation, ω ($= 2\pi f$) is the perturbation frequency, k ($= 2pi/\lambda$) wavenumber, g is the gravitational constant, γ is surface tension, ρ is density, and h_0 is the fluid height. For deep water waves, the fluid height dependence is essentially negligible. Generally, related to the forcing amplitude, subharmonic waves at half the forcing frequency are observed. When the driving amplitude becomes large, droplets and wave breaking may occur, as surface tension is unable to restore the surface. Due to nonlinearities in a standing Faraday or capillary waves, a net horizontal (along the wavefront) particle transport on the surface of the wave also exists. This is due to differences in drift motion over one wave period and is defined as the difference between the average Lagrangian and Eulerian velocities. It is known as Stokes drift and can also be important for mass transport (additional convective motion) [11, 12]. On a 2D free surface with a standing wave pattern such as a capillary wave, this drift is not in a singular direction and rather follows random motion due to the nonlinear effect. These processes are forcing amplitude dependent for Faraday waves. The addition of this nonlinear term in the advection-diffusion equation is sometimes combined with the molecular diffusion term as an 'anomalous diffusion' source [6].

This work utilizes a nanosecond (ns) pulsed blade electrode to liquid water plasma configuration to study the effects of the acoustically perturbed Faraday interface on plasma morphology and reactive species transport to solution. Reactive species transport is probed using a model contaminant dye (methylene blue), where discoloration is due to interactions with reactive species [7]. Simulations with *nonPDPSIM* were also conducted, matching experimental conditions, to probe localized conditions on the single pulse time scale (excluding convective motion). The goal of this work was to produce uniform surface perturbations such that the interfacial perturbation surface morphology affects on the discharge could be studied without the full array of chaotic turbulent effects (ancillary processes including bulk motion from turbulence).

2. Setups

2.1. Experimental setup

The experimental setup is shown in figure 1. In these experiments, a ns pulsed plasma is generated (with the low power EHT) in open air above a water dish on top of a speaker. To vary interfacial morphology in a controlled manner, Faraday waves were acoustically driven over a range of driving frequencies to vary the size of the surface structures associated with the waves. These Faraday waves, or capillary waves, at high driving frequencies generate standing waves that allow

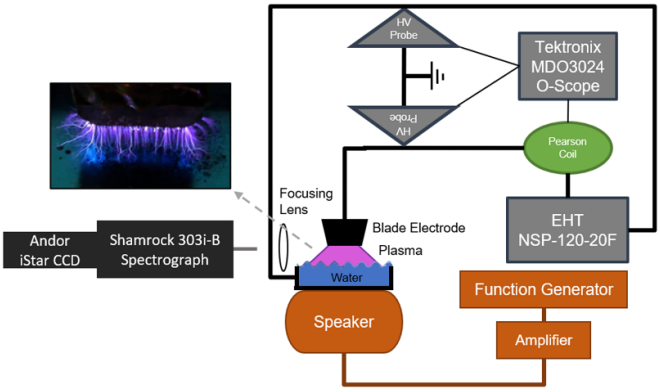

Figure 1. Experimental setup for Faraday/Capillary wave experiments. Note that the EHT ns pulser can be produce positive or negative streamers by biasing the blade electrode with the high or low voltage lead.

for control of the interface morphology without introducing appreciable bulk mixing [13]. Faraday waves are driven at the free surface, and a thin layer of water is used to prevent complete viscous dampening as the sound wave propagates through the liquid. The smallest wavelength attempted aimed to approximate the smallest physical length scales of turbulent flow (Kolmogorov eddy size) [14].

By altering the speaker frequency and amplitude, water waves of varying wavelengths can be driven, shown in figure 2 with measurements in table 1. The speaker (BMS 4592) was driven by a sinusoidal function generator (PASCO PI-8127) and an amplifier (Blaupunkt THA475PnP). The function generator was powered with a DC supply (Kikusui PAD 55-10 L). Due to limitations in controlling the wave amplitude (that could be mitigated by a different driving force, such as a vertical oscillator), the driving amplitude was simply chosen as the lowest driving amplitude to produce waves. This was done to ensure no wave breaking occurred (with a transition at much larger forcing amplitudes). Wave heights and frequencies were roughly inferred using a camera (figure 2) imaged at 30 degrees relative to the liquid.

The water acts as a dielectric barrier to allow for streamer formation from the steel blade electrode (0.38 mm thickness, 15.8 mm width) to the liquid, contained in a plated steel tin of 95.25 mm by 60.33 mm (W) by 19.05 mm (D). 20 ml of water gave a height of around 4 mm, thin enough to ensure viscous dampening did not prevent wave formation. A large container was chosen for twofold reasons: 1) it allowed for a large enough sample collection volume for instrumentation, and 2) effects from the walls could be neglected.

In these experiments, the ns pulsed plasma had the following variables for control: pulse frequency, applied voltage, electrode spacing, and discharge polarity. By switching the blade polarity, positive and negative streamers were formed. This was done partially to ensure matching with simulation results, which were produced only with negative polarity discharges. In all cases, the pulse width was set to 180 ns. DI water (Milli-Q), or DI water spiked with around 20 ppm methylene blue (MB), were used as the liquid dielectric. MB acts as a model contaminant to assess transport of plasma generated reactive species. Calibrated UV–Vis spectroscopy (Thermo Genysis 150) was used to assess decoloration rates of the dye using Beer's law at 609 nm [15]. As MB is not a surfactant and thus does not alter the surface tension of the solution, the Faraday waves generated were expected to match those of DI water. Power was estimated with current–voltage waveforms and did not appear to change significantly with different surface perturbations (around 1 W for 2.5 mm gap, 14 kV, positive polarity, and 100 Hz), only with other discharge conditions.

Optical emission spectroscopy (OES)(Andor iStar CCD and Shamrock 303i-B spectrograph) was conducted to probe non-spatial or temporally resolved plasma properties. OES measurements were made exclusively with positive streamers.

A brief experiment to look at discharge morphology was attempted. However, due to the random streamer formation it was difficult to precisely observe effects of the capillary waves. Instead, to promote a single streamer, a needle electrode replaced the blade electrode and the discharge was imaged (Andor Sona sCMOS). The total propagation distance of the streamers was estimated with a MATLAB script based on the emission area collected by the camera for different discharge conditions. In this way, the discharge propagation area could be compared to models (*nonPDPSIM* discussed later).

The driving frequencies (from the driving source) used for further experiments and modeling are listed in table 1, along with the capillary wavelength and amplitudes.Theoretical and experimentally observed wavelengths are compared in figure S1. The lowest amplitude in which a wave occurred was chosen, as at certain resonant frequencies or high driving amplitudes the waves could break and produce undesirable droplets and bubbles. In this work, the smallest wavelength experimentally driven lie in the range of 100's μm, which is larger, although assumed to be a reasonable approximation, for the small eddies produced in turbulent flow (at the Kolmogorov scale) [14, 16, 17]. In general, the longer perturbation wavelengths had larger driving amplitudes. Edge effects (surface tension) with the container could be neglected as the container was much larger than any wave produced.

2.2. *nonPDPSIM* Simulation Setup

A 2D plasma simulation code *nonPDPSIM* was additionally used to understand the local plasma dynamics at play over a single discharge event [18]. *NonPDPSIM* is a 2D finite-volume multifluid model that solves for electromagnetic field variations, neutral and charged species dynamics, and chemical kinetics on an unstructured mesh grid. Charged species fluxes are obtained using Scharfetter-Gummel method, while neutral and charged species densities are obtained from solutions to the mass, momentum, and energy continuity equations. Volume and surface space charges are obtained from a fully implicit solution to Poisson's equation, updated

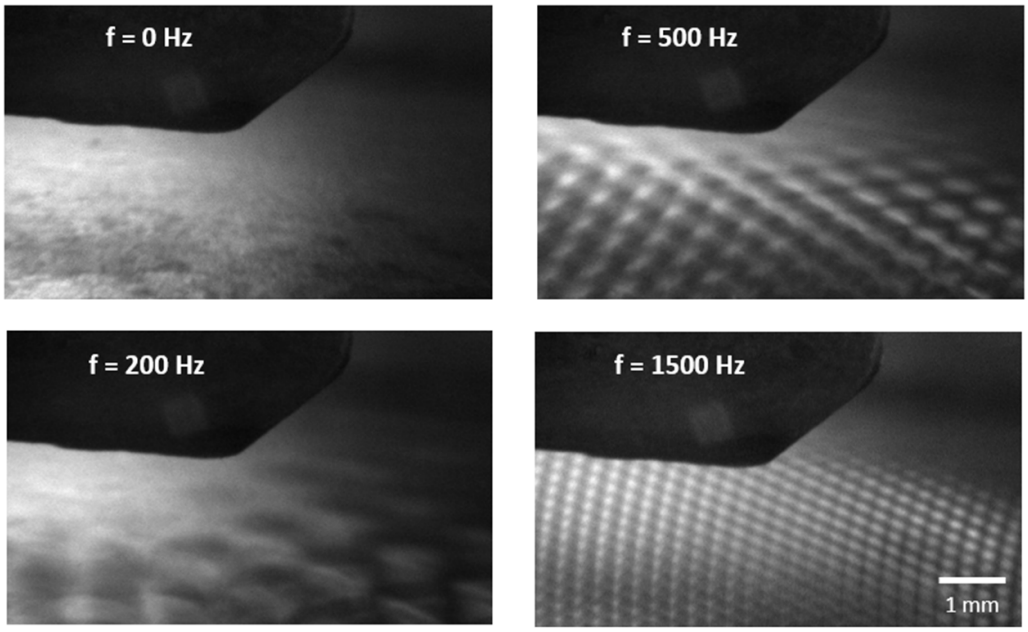

Figure 2. Images of capillary waves used for experiments, for the flat case and three driving frequencies, noting that an increase in driving frequency decreases the capillary wavelength.

Table 1. Driving frequency (by the speaker) and the resulting capillary wavelengths and heights.

Driving frequency (Hz)	Capillary wavelength (mm)	Wave height (mm)
0	—	—
200	1.37 +/− 0.10	0.54 ± 0.05
500	0.78 +/− 0.04	0.33 +/− 0.04
1500	0.35 +/− 0.03	0.14 +/− 0.02

concurrently with changes to the space charge via a Newton–Raphson method. Simulations included separate treatment of bulk (thermal) and secondary (non-thermal) electron species. The bulk electron temperature is determined by an implicit successive-over-relaxation solution of the electron energy conservation equation, which is updated after each iteration of the charged particle species and electric potential as described above. Electron-impact rate coefficients are calculated by first creating lookup tables for solutions to Boltzmann's equation over the range of E/N in the simulation. Electron impact rate-coefficients, as a function of electron temperature, are extracted from these tables, interpolated to the electron temperature in each simulation cell. Solvated electrons are assumed to have a constant temperature of 0.03 eV. Reactions between gas phase electrons and liquid H_2O was facilitated by a surfactant model [18]. Secondary electrons are emitted from both solid and liquid surfaces employing an energy independent model. A secondary electron emission coefficient of 0.10 was employed on all surfaces for all ion species. Secondary electron motion is tracked kinetically, where secondary electron impacts and reaction kinetics are computed employing a Monte-Carlo model utilizing the same reaction mechanism as the bulk electrons. Photoionization of N_2 and H_2O was captured in the gas phase and gas/liquid phases, respectively where radiation transport is computed from solutions to Green's function, solved concurrently with the Newton–Raphson method noted above.

The setup is shown in figure 3 for the flat water case. The perturbed wavelengths cases roughly correspond to the experimental values listed in table 1, with slight adjustments to make the alignment at the container edge equal. In this case, the number of wave structures created is used to indicate the wavelength (n00 is flat, n08, n16, and n32 are decreasing wavelengths, respectively). The n00 case was flat, the n08 case had a $\lambda = 1500$ μm and $h = 600$ μm, which corresponds to the 200 Hz driving frequency, the n16 case had a $\lambda = 750$ μm and $h = 300$ μm, which corresponds to the 500 Hz driving frequency, and the n32 case had a $\lambda = 375$ μm and $h = 150$ μm, which corresponds to the 1500 Hz driving frequency. The average water height remains the same as the n00 case for all perturbed simulations.

In all cases, the top steel electrode (0.5 mm radius tip) is powered over a liquid water (assumed deionized with a conductivity of 5 μS cm^{-1}) in a grounded metal dish of 1.2 cm radius. External outlet boundaries were grounded in order to provide a boundary condition for the Poisson solver. A low flow (250 sccm) humid air flow condition between the inlet and outlet is established to aid in simulation convergence (experiments were conducted with no gas flow other than room flow). The humid air had a composition of $N_2/O_2/H_2O$ =

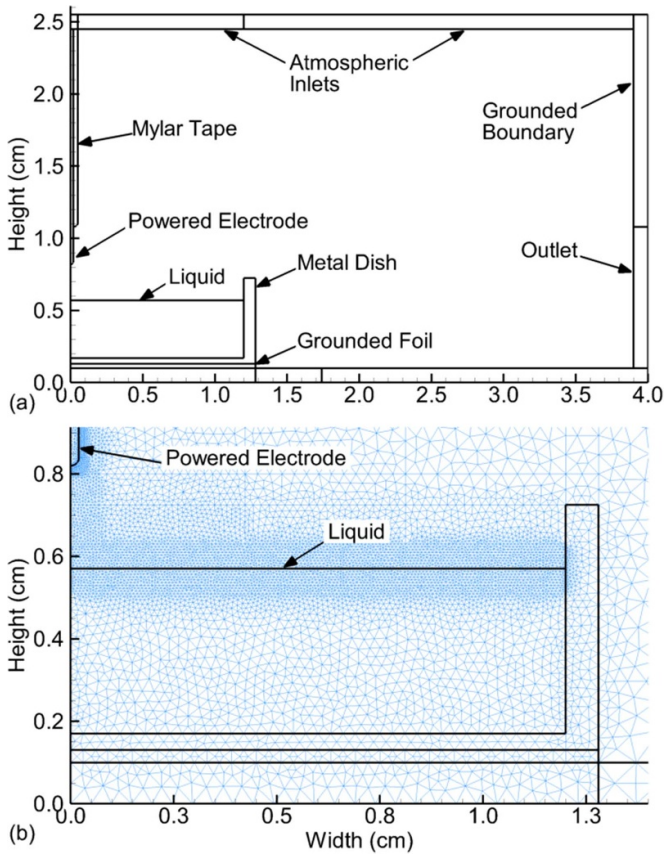

Figure 3. Simulation (a) setup and (b) meshing.

0.795/0.2/0.005. Prior to simulation of the plasma dynamics, a neutral flow-field was computed within the same simulation geometry employing a Navier–Stokes solver. The flow field was solved for 10 ms prior to the discharge for each simulation. For the flow boundary conditions used here, 10 ms was found to be suitable to reach convergent flow fields and allow for equilibrium water vapor pressure above the water surface. In this setup, simulations are conducted essentially from the side of the blade from the experiments, to simulate a single streamer propagation. The simulation can extend infinitely in the z direction, thus making it an approximation for the blade electrode.

A symmetry boundary condition is placed at the center point. The total liquid volume is 9.6 ml, about half that of the experiment. With the acoustic perturbations, the center of the peak wavelength is at the symmetry boundary condition (closest to the electrode). The mesh surrounding the liquid has uniform node spacing around the perturbed liquid state to improve fidelity of fluxes to the interface. The resolution varied between 0.04 mm/cell at the interface to 1.0 mm/cell in the ambient air to the right.

The voltage applied (-14 kV) to the top electrode was negative due to difficulties arising when simulating the positive discharge. Otherwise, similar conditions were used as the experiment (2.5 mm gap width, 180 ns pulse duration). The simulation was tracked up to 1000 ns to determine afterglow species concentrations. The pulse had a 5 ns rise and fall time.

In order to compute the effective surface area increase in this simulation (due to the Cartesian geometry of the simulation effectively giving a series of parallel waves), the following equation was employed:

$$L = \int_0^{2\pi} \sqrt{1 + \frac{\mathrm{d}y}{\mathrm{d}x}^2}\, \mathrm{d}x \tag{2}$$

where L is the effective curve length for a single wavelength, dx and dy represent components parallel to the propagation parallel (x axis) and amplitude parallel (y axis). For any perturbation wavelength, the effective length is scaled by 1.216 relative to the flat case. This is because the amplitude and wavelength scale proportionally in this case, leading to the same integration factor.

3. Results

3.1. Bulk plasma OES

In order to assess the response of the bulk plasma with the introduction of the interfacial Faraday waves, OES was used. In this case, driving frequencies were increased to the maximum textured wave structure (minimum wavelength) given the driving amplitudes capable by the acoustic excitation device, in this case at 1500 Hz. The plasma was produced with positive polarity streamers (liquid cathode). A parameter sweep was conducted between the flat and high frequency cases with the low power EHT ns pulser, in this case for pulse frequency (100–4 kHz), voltage (10–18 kV), and gap width (1, 2.5, 5 mm).

Due to the standing wave structure of the water and the movement of the streamers, it was not possible to measure local plasma ionization waves. Rather, the OES represented a spatiotemporal average in response to changes in the bulk discharge. Results are given for the total plasma emission (electrode to water) that is temporally averaged over many discharge pulses. A preliminary investigation for the E/N, based on nitrogen emission ratios [19], found a general value of 300–450 Td, with no clear patterns with any parameter sweep (small emission intensities of the FNS made this analysis difficult for 1 kHz and less). However, this observation is similar to the average streamer fields found in other work [20]. Additionally, Stark broadening was used to estimate the electron density from the H_α emission line [21]. Average values of $1\text{–}5 * 10^{22}$ m^{-3} were determined . However, this line only appeared at high frequencies above 1 kHz (not all cases—possibly due to low emission intensity or the lower gas temperature reducing water vapor concentration), and thus, again, a trend could not be found.

Gas temperature was estimated with massiveOES software for the N_2 SPS emission line [22]. Figure 4 shows the average gas temperature as a function of discharge frequency. The gas temperature ranged from around 400 K at 100 Hz to around 750 K at 4 kHz. In this figure, the temperatures are averaged across the other parameter sweeps, though it should be noted that the other parameters had a very limited effect on

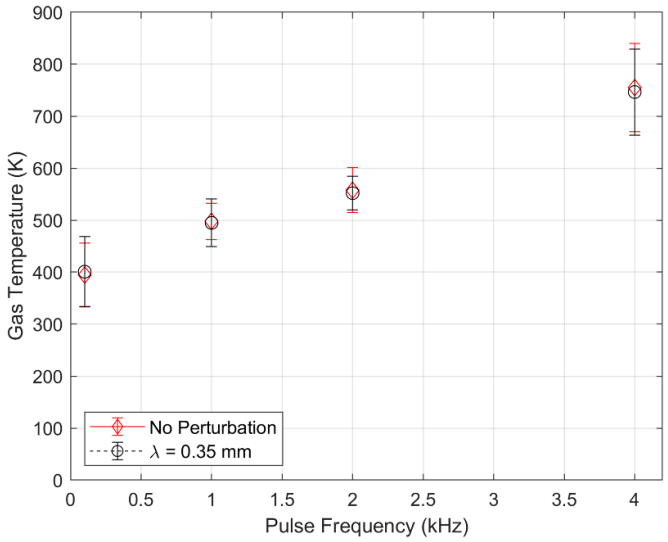

Figure 4. Gas temperature estimations including standard deviation over multiple measurements as a function of discharge frequency from positive streamer discharges with and without shortest wavelength Faraday wave perturbations.

the bulk temperature. Essentially, it was found that of the parameters swept, bulk temperature was solely dependent on frequency. This makes sense, as the higher frequency can lead to memory effects between discharge pulses as well as having a higher power deposition into the same gas volume [23]. Additionally, it is notable that the bulk gas (rotational) temperature remained constant with or without the addition of capillary waves, providing evidence that the streamers propagating from the electrode to the water surface do not change appreciably when the liquid surface changes. Although OES was not conducted with negative polarity discharges or with other perturbation frequencies, a similar trend would be expected.

3.2. MB decoloration

Initial MB decoloration testing were carried out with discharge pulse frequencies ranging from 1–4 kHz, all with positive polarity. The decoloration pseudo first-order rate constants did not vary with perturbations (figure S2), rather only changing with pulse repetition frequency (from around 0.2 min^{-1} at 1 kHz to 0.4–0.5 min^{-1} for 2–4 kHz. Since the plasma parameters remained unchanged (as based on OES data), it would be expected that at a minimum the enhanced contact surface area provided by the capillary waves should play a role in the transport (and therefore decoloration). It is postulated then that EHD forces induced by the plasma, due to surface charging a polarizable dielectric such as water, could be negating any effects from the externally generated capillary waves. As demonstrated by ANSYS Maxwell in figure S3, an electrostatic field solver, at standard conditions (2.5 mm gap and 14 kV), a clear enhancement of the electric field can be seen when comparing a driving frequency of 1500 Hz to the flat surface.

A sinusoidal or pulsed electric field can bring about deformations at the liquid surface [24]. Robinson has demonstrated these surface wave formation with an AC induced electric field [25]. Residual surface charge can alter the propagation of any surface charges such as surface ionization waves (SIWs) [26].

The issue here is that these capillary waves are naturally excited with the pulsed power supply used in this work. The dispersion relation for a perfectly conducting liquid is given in equation (3) [24, 27]. Similar to the generated Faraday waves, an electric field component E can drive surface perturbations based on the excitation frequency,

$$\omega^2 \approx \left(\frac{\gamma}{\rho}k^3 - \left(\frac{\epsilon_0 E^2}{2\rho}\right)k^2\right). \tag{3}$$

The generated wavelengths based on the excitation frequency are shown in figure S4 for the otherwise same conditions used to estimate the acoustically driven Faraday waves, where the bulk electric field is estimated from the Maxwell simulations (on the order of $6*10^6$ V m^{-1}). Notably, these subharmonic oscillations produced via acoustic excitation are approximately equal those of the plasma generated waves at the electric fields of interest when the plasma is excited at the frequencies tested,

$$\omega = 2\pi f_{\text{obs}} \approx \pi f_{\text{exc}}. \tag{4}$$

Thus, the wavelengths produced the kHz discharge are close to those produced by the kHz acoustic excitation,

$$\lambda_{\text{plasma,kHz}} \approx \lambda_{\text{acoustic,kHz}}. \tag{5}$$

Since these naturally excited waves provide a similar surface perturbation to those excited acoustically, without the lack of contrast in frequency the impact of the externally generated acoustic wave is not discernible. Thus, the high frequency driven plasma cannot be used to compare surface perturbation effects. A lower frequency (in this case 100 Hz) must be used such that the wavelength of the plasma generated waves is much longer than those produced acoustically (order a few mm for the EHD driven waves). The addition of high frequency pulsed (or sinusoidal) electric fields can distort the liquid surface, enhancing transport of the reactive species transport to the liquid. This high frequency perturbation should be included in mechanisms for plasma liquid interactions. The next section discusses the results of both positive and negative streamers discharging at 100 Hz for MB decoloration. It should be stated once again that no bulk plasma modifications were observed using OES at this frequency.

3.2.1. Positive and negative streamers at 100 Hz. The results of the 100 Hz MB testing is shown in figure 5, for both positive and negative streamers. A key result observed here is that in both positive and negative streamer polarities, an enhancement on MB decoloration rates can exist with the addition of Faraday waves. It should be noted that the starting concentration hovered around 15 ppm and exhibited first order

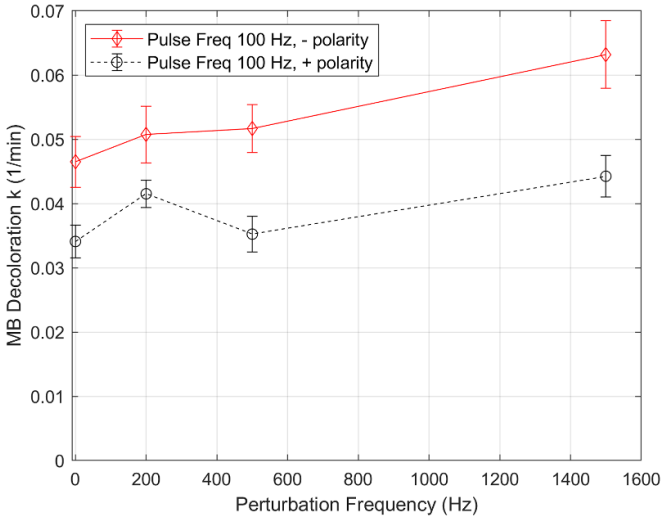

Figure 5. MB decoloration rate (first order) for positive and negative streamers at 100 Hz and different perturbation frequencies, error bars represent 95% confidence for fit.

decoloration characteristics. A few experiments were conducted (not shown) with higher starting concentrations approaching 15 ppm, and in these cases, zeroth order (linear) decoloration was observed initially. Hence, it is apparent that there is a plasma species limited regime at high concentrations, an effect that has been observed in other work [28]. A transport limited regime appears below, giving pseudo first order kinetics. In this case, there is an abundance of reactive species present to react with the more limited MB molecule.

Another note is that MB is not a surfactant [29]. This means that the surface tension and thus acoustic perturbation characteristics would not be expected to differ much from those produced in DI water. It also means that while the concentration of MB at the interface will exhibit a concentration gradient as it is being degraded, it will not preferentially form this gradient while being left in solution.

The estimated power around 1 W (at 100 Hz) did not change significantly between the positive and negative polarity discharges, or with the capillary wave formation. The estimated power did consistently increase with time (around 0.1 W through the duration of the 20 min tests), likely due to the water conductivity increase. Since the power does not change between these modes, it is not hypothesized to play a role in the observed decoloration rate constants.

In both discharge polarities, an increase in the first order kinetic decoloration rate is observed when a perturbation is included, particularly at the highest frequency (lowest wavelength) waves. This trend is consistent for both positive and negative electrode polarities, though the rates had both a polarity and frequency dependence. First, the negative polarity discharge exhibited higher decoloration rates in all cases. Second, a noticeable increase in the rate constant was apparent for the 200 Hz perturbation (largest wavelength).

The peak at the 200 Hz driving wave may be due to some sort of plasma enhancement. In this case, the EHD driven wavelength at 100 Hz and the acoustic driven capillary wave were of the same magnitude, thus potentially interfering with each other. Additionally, the height of the longer wavelength perturbation is larger, which can improve electric field enhancements. As shown later, the same rate increase appears for the total emission area of the positive discharge, indicating this may be a consequence of larger interfacial contact area.

Interestingly here, the negative emission consistently exhibits higher decoloration rates. The emission area of the negative streamer appears spatially smaller than that of the positive streamer configuration, as discussed in later sections. This means the total interfacial contact area is likely lower. However, the explanation here may lie in the reactive species generated from a positive vs negative streamer emission, as well as the role of the interfacial sheath accelerating charge into the liquid. A negative polarity discharge has been shown to exhibit significantly higher reduction properties due to the increase in solvated electron densities (accelerated into the water). Radical species concentrations in the plasma may depend both on the polarity of the discharge and preferentially to the pH (positive polarity) and solution conductivity (negative polarity) [30].

The solvated electrons that play a role in compound reduction may help explain why the negative streamer exhibits higher decoloration rates. Similar to oxidation decolorizing MB species, the reduction of MB forms a colorless compound leucomethylene blue, LMB [31]. Additionally, the negative streamer is more electron impact driven rather than photoionziation driven (except for the reverse wave), and thus can drive higher temperatures. The improvement of MB dye decoloration in negative polarity streamers relative to positive polarity has also been observed in Hamdan [32], which they attributed potentially to larger measured peroxide formation rates, although exact mechanisms remain inconclusive.

While the polarity of the discharge may explain why the rate constants differ between positive and negative streamers, it does not explain the increase in decoloration rates when an acoustic perturbation is added (and why, for that matter, the smaller perturbations have larger impacts). For this, two possibilities are considered. One is the local plasma morphology and surface contact area, which drive local transport into solution and the size of the wave structure. This includes possibilities such as local changes in reactive species densities due to local electric field enhancements or reductions at the peaks or troughs, respectively (surface charging). The second possibility is hydrodynamic effects due to a spatially and temporally moving interface. While difficult to ascertain the absolute magnitude of each effect due to coupling, the next sections discuss some of the possible impacts on transport for to explain the MB decoloration rate.

3.2.2. Surface area. One obvious consideration is the total surface area presented to the reactive species at the interface. Particularly important for longer-lived species that can persist outside of the plasma on time, a higher contact area will lead to

more transport into the solution. One way to estimate this surface area increase is through assuming a simple step function wave, shown in equation (6) [13].

$$F_{\mathrm{SA}} = 1 + \frac{4H}{\lambda} \tag{6}$$

where F_{SA} is the surface area enhancement ratio, H is the wave height, and λ is the perturbation wavelength. This represents the maximum surface area increase possible given the wavelength and wave amplitude. As calculated (see figure S5), the surface area increases by a factor of just over 2.5 relative to the flat surface, and is consistent across the waves. This increase is likely consistent because the amplitude of the largest wavelengths is also the largest. Although there is an increase in MB rate constants, it does not increase equally for each capillary wavelength, indicating this is not the primary driver for the rate constants observed (though it likely still plays a role).

3.2.3. Stokes drift. Hydrodynamic drift velocities also may help explain the observed rate constant increase. While there are convective motions driven by the plasma (ionic wind and Marangoni stresses) [4, 33], this section focuses on surface motion from the waves themselves.

A traveling wave has a net surface velocity given by Stokes drift [8, 34], which can assist in surface mass transport by providing convection near the interface. This Stokes drift is a net Lagrangian surface motion and is given in the following equation [34]:

$$u_{\mathrm{sd}} = v_{\mathrm{p}} (Ak)^2 \cosh\left(2k\left(h_z + z\right)\right) / \left(2\sinh^2\left(kh_z\right)\right). \tag{7}$$

In this equation, u_{sd} is the Stokes drift velocity, v_{p} is the wave phase speed, A is the wave amplitude, k is the wavenumber, h_z is the liquid depth, and z is the distance from free surface (negative, $z = 0$ indicates the free surface). Clearly, the Stokes drift velocity is a strong function of the depth, and is highest at the liquid surface. Eventually, for a deep enough wave, there would be almost no net drift velocity. If the Faraday waves produced in this experiment were traveling waves, the Stokes drift velocity could approach 1.5–3.5 m s^{-1} (figure S6), which would have important impact on interfacial renewal and lateral transport of the reacted liquid away from the interface.

This assumption of traveling waves, however, cannot be used for the experimental conditions of interest. For a perfect standing wave, such as an ideal Faraday wave, this net surface velocity over a complete cycle is zero. However, due to the nonlinear nature of real Faraday waves, due to dissipative terms and small velocity perturbations, such as in this setup, random walk processes can provide a net convective motion of particles at the surface of the waves [12]. This additional convective motion, sometimes called stochastic or fluctuation Stokes drift or anomalous diffusion [11], acts to provide enhanced transport and interfacial replenishing. This random walk primarily depends on the wave amplitude and frequencies, both correlated to forcing processes [11]. When the forcing amplitude becomes large enough and disordered, these Faraday waves effectively act like 2D turbulence at the surface (with a similarity in energy spectra) [35]. The effective diffusion term includes advective motion and molecular diffusion, and can be greatly enhanced by these Faraday waves. In fact, Mesquita found the effective diffusion coefficient for Faraday waves similar to those produced in this work can be 10^3 larger than molecular diffusion alone, demonstrating that these stochastic surface drifts can play a major role in interfacial transport processes [36].

The ensemble averaged Stokes drift is given in Mesquita can be used to estimate the convective terms for the capillary waves produced in this work [36]. A closer approximation to the magnitude of surface velocities can be estimated with this fluctuating Stokes drift model. In this model, the ensemble averaged Stokes drift $\langle u_{\mathrm{sd}}(z)\rangle$ for a random-wave field is given in the following:

$$\langle u_{\mathrm{sd}}(z)\rangle = 2\int F(k)\,\omega k e^{2kz}\mathrm{d}^2k \tag{8}$$

where the 2D wave spectrum $F(k)$ is normalized to the mean square surface displacement $\langle H^2\rangle$,

$$\int F(k)\,\mathrm{d}^2k = \langle H^2\rangle. \tag{9}$$

Assuming an an isotropic rectangular surface, and a displacement spectrum consisting over a narrow peak Δk around k_0, the wave spectrum is given in the following, and can be used in the equation (8) to solve for an average surface drift velocity for the Faraday waves,

$$F(k) = \frac{\langle H^2\rangle}{2\pi k_0 \Delta k}. \tag{10}$$

The calculated drifts in this disordered regime are on the order of 15–35 mm s^{-1} for the lowest and highest frequency perturbations, respectively, which is similar to the surface drift velocities found in the literature [13, 35, 37]. Some consider this drift a 2D turbulence, but even still measured velocity fluctuations averages in the same mm/s-10 s mm s^{-1} range for a Faraday wave field [35]. It should be noted this drift is not uniform along the surface (hence a "turbulence" description), but should have a net impact on the average convective transport of reactive species away from the interface (and contaminants toward the interface). In addition, processes that reduce the surface tension, like the presence of surfactants, will alter this drift motion. Viscous dissipation in the boundary layer region can also give rise to these nonlinear convective motions.

A simple comparison of the fluctuating Stokes drift and diffusive flux can indicate the relative importance at various fluid depths (see Vasilev for laminar convective flux [38]). Since transport of plasma generated reactive species is limited to a thin interfacial layer, the depth at which convective forces are important can help explain transport phenomenon

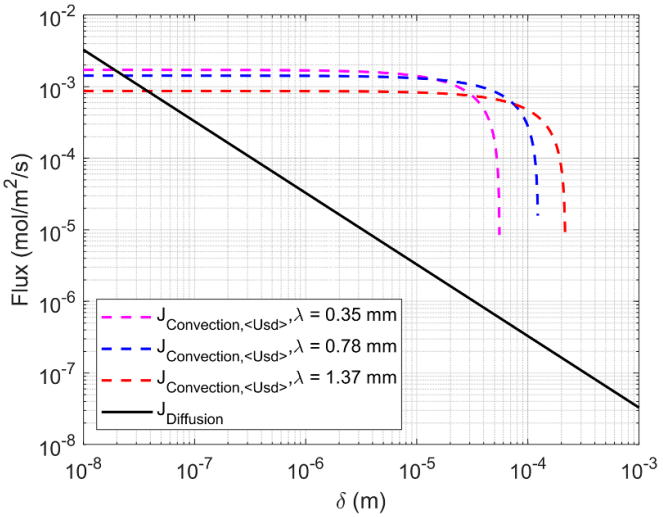

Figure 6. Estimated convective and diffusive flux based on average surface drift at different water depths.

and observed MB decoloration. Assuming a constant concentration gradient, the diffusive flux J_{diff} will be proportional to this concentration gradient (DC/δ), which is linear with respect to the fluid depth. The convective flux J_{con} would be proportional to the average drift velocity at the fluid depth and concentration. Assuming a 15 ppm concentration of MB ($=$ 0.047 mol m^3) and a diffusion coefficient of MB in water of $0.7 * 10^{-9}$ $\text{m}^2\,\text{s}^{-1}$ [39], the relative convective and diffusive fluxes can be calculated. Results are shown in figure 6 for depths of 10 nm to 1 mm.

A few interesting observations can be concluded here. First, the smallest wavelength has the highest average surface drift. Second, the convective drift estimated from this method does not penetrate further than a few hundreds of μm. Third, at depths approaching the plasma liquid interface, where the bulk of reactive species are transported (and then chemically reacted), diffusive and convective fluxes are of similar magnitudes, with the crossover point on the order of 10's nm. Since these fluxes are similar at the interfacial solution depth, the convective surface motion generated by the Faraday waves can likely play a role in the observed decoloration rates. Furthermore, the impact of these hydrodynamic motions is highest for the smallest wavelength (highest driving frequency), following the observed trend of increased rates with driving frequency.

3.3. Streamer propagation distance

Finally, the propagation of the streamers is observed noting that larger streamer propagation provides an increased area for mass transport. In this case, the blade electrode was replaced with a needle and discharged at the same conditions (100 Hz pulse frequency, 14 kV discharge voltage, and 180 ns pulse width) at various gap distances and polarities. With a high enough applied electric field, the streamers tended to follow the interface and propagate as SIWs. In this case, the total emission at the water surface was captured in long exposure imaging (averaged over many discharge events), similar to that observed in Hamdan but over many discharge events [32]. Anything below 3% of the maximum emission intensity is assumed to be background, as this was found to provide a stable emission area. Averaging over multiple events provides uncertainty, and all the data was normalized to the largest emission area of 200 Hz perturbation frequency, 2.5 mm gap, positive polarity.

Figure 7 shows the relative emission areas for three cases: 2.5 mm gap of positive and negative polarity and 1 mm gap with negative polarity. As mentioned previously, a increase in induced surface area occurs at the 2.5 mm gap, positive polarity case, which corresponds to an increase in MB decoloration rates. As will be discussed in with ionization wave model, it is possible that the SIW is able to 'hop' over the larger amplitude waves, allowing it to propagate relatively further in this case. The larger needle to water gap, particularly in the negative polarity case, sees less influence of discharge propagation area with perturbation. This is likely because the electric field is not strong enough to continue the propagation of the streamer as a SIW, thus reducing a significant amount of emission area. Hence, a 1 mm gap was tested for the negative polarity case, and the expected increase in surface area with capillary perturbations was observed.

Positive streamers have been shown to propagate further relative to negative streamers due to enhanced space charge induced at the streamer head (electron impact vs photoionization) [40]. This may help to explain why the positive polarity streamers had much larger propagation areas (around doubling for the same gap distance). Interestingly, this propagation area likely plays a reduced role in the decoloration rates observed, given that the positive streamers had both a larger area and lower decoloration rates. This highlights that the reduction processes at play from the negative streamer emission may be critical to the rate constants observed.

Finally, with regards to the capillary waves and decoloration rates, it is clear that surface area of the discharge emission follows a similar pattern to the rate constants, in that the larger emission areas have larger decoloration. This is the expected outcome, although there are still peculiarities that cannot be explained by these factors alone. As it has been stated, the local relative emissions can also alter local transport of reactive species, and all the data presented herein represents temporally and spatially averaged data. To get local resolutions of interest, modeling must be used to help explain these observed conditions.

3.4. nonPDPSIM Simulation results

The first notable result of the simulations is the E/N during the pulse. Shown in figure 8 at the end of the discharge pulse for the n00 (flat), n08 (200 Hz equivalent), and n32 cases (1500 Hz equivalent), there is a clear field enhancement near to peaks and decrease near the troughs. This localized enhancement is most pronounced for the lowest perturbation wavelength

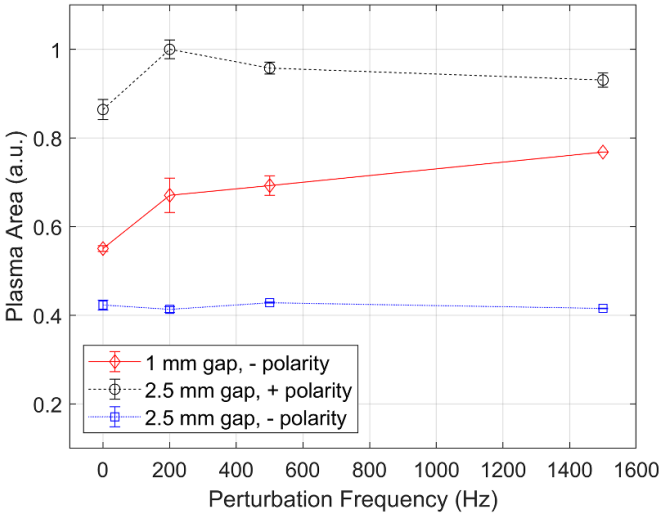

Figure 7. Emission area for a needle-to-plane discharge at different perturbation frequencies, gap spacing, and discharge polarity, with error bars representing standard deviation of three long duration images.

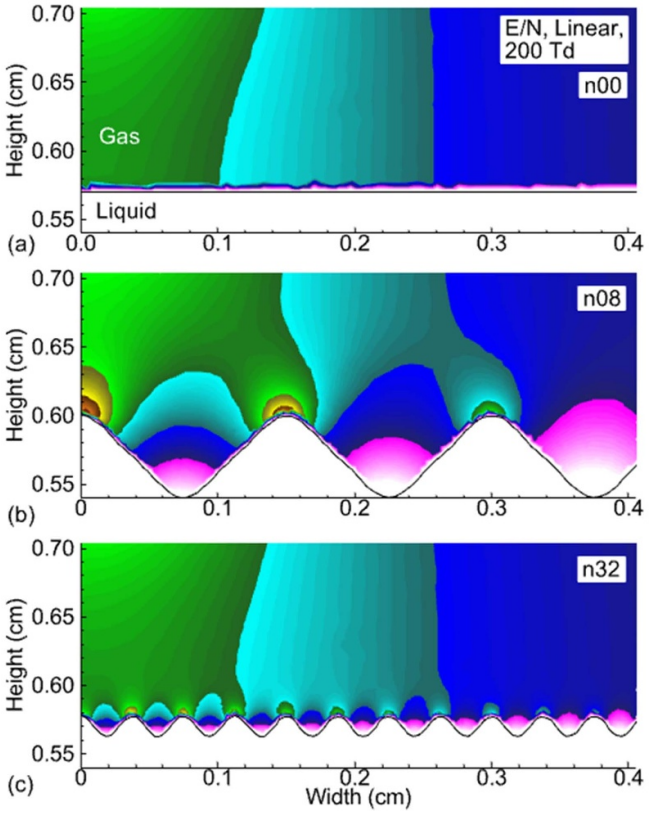

Figure 8. Reduced electric field E/N for (a) the flat case, (b) a mid-wavelength perturbation, and (c) the smallest perturbation wavelength showing enhanced fields at the peaks.

(n32), which makes sense because in this case, the wave amplitude and thus polarization is largest. In the case of an infinitely small wavelength, the flat E/N should be reproduced. It is also notable that the bulk field does not change much, consistent with experimental estimations of bulk emission properties.

The polarization wave peaks also exhibit a higher surface charge density, which enhances the E/N. The discharge path is as follows: for the negative discharge, an electron impact driven initial streamer is formed. In the n00 flat water case, the discharge propagates to the surface of the water and then outward as a SIW. Due to the polarization of the water when a perturbation is introduced, the surface of the wave structure following the ionization provides photoionization that precedes the next discharge. This induces the ionization wave to preferentially hop between the right surface of the wave structure (as the discharge propagates from left (electrode) away). The photoionization drives a reverse, positively driven ionization wave. This pre-seeding photoionization is due to the locally enhanced fields near the tip.

The IW hopping phenomenon and reverse ionization wave has been both simulated and experimentally observed with plasma propagation over channels filled with water [41]. This further highlights the complex geometry that can locally modify the attachment points of the plasma or the propagation of SIWs. These studies also note the impact of polarization of the water on the discharge propagation mode. Local, high radical fluxes are driven at these streamer propagation points, leading to surface morphology dependant fluxes along the wave surface. In the troughs, the addition of water vapor and lack of strong ionization leads to much less flux. The flat surface case sees the expected SIW distribution highest just below the discharge and slowly falling off.

An easy visual representation of the change in fluences to solution are shown in figure 9 for all perturbation cases, as well as the flat surface case. This fluence is the integrated time dependent normal flux of a species at the interface over the discharge pulse and the afterglow for the full 1000 ns simulation domain. The fluence gives an estimation of the total generated species impinging at a particular point on the liquid surface, assumed to be stationary through the simulation domain period. In this, the total electron fluence and hydroxyl radical fluence are shown along the liquid surface as propagating in the x direction. Additionally, the surface of the perturbation systems has been scaled down by the factor of 1.216 to account for the sinusoidal path length, discussed previously. The third panel gives a visualization of these fluences relative to their respective wave structures.

Clearly, there is a nonuniform distribution of radical species (as well as other longer lived species not shown here) across the interface. The concentrations tend to increase in regions of high plasma excitation sources and decrease in low sources (valleys). The localized topographical structure is clearly impacted by the perturbation wavelength. Although the distribution relative to the location varies from well above the n00 case and well below, the total area (total fluence) can be larger for the perturbed wavelengths.

Finally, as demonstrated by the species fluences, the discharge propagation region is spatially larger on the perturbed surface. This matches well with the experimentally determined emission distance shown in figure 6.

To highlight how the simulations compare to the experiment, the integrated surface fluence (figure 6) can be compared

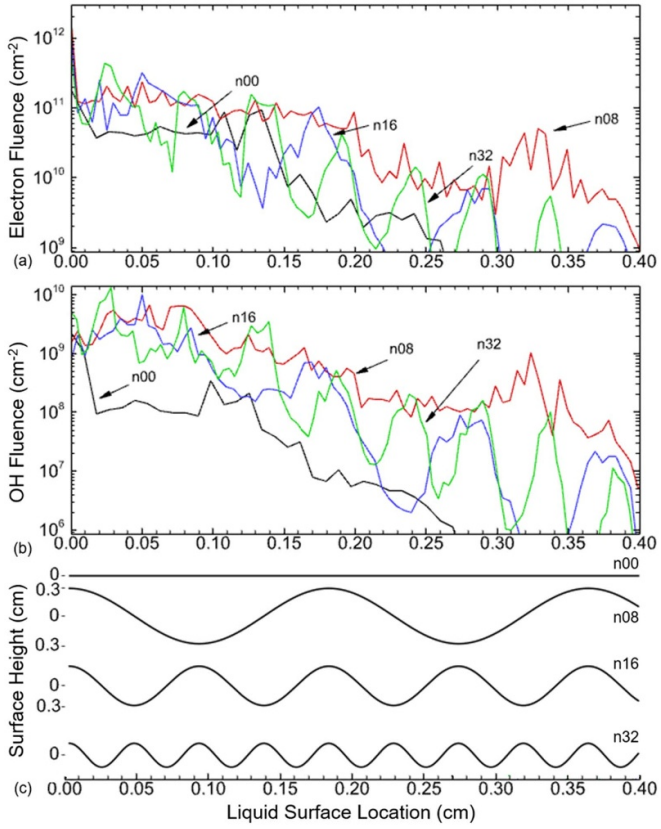

Figure 9. Fluence over the simulation time for (a) electrons, (b) OH for different perturbation wavelengths, and (c) surface perturbation patterns for each case.

to the decoloration rate constants measured with the negative polarity discharge. The experimental rate constant increases roughly 9%, 11% and 36% for the perturbed cases (at 200 Hz, 500 Hz, and 1500 Hz) relative to the unperturbed experiments. The total fluence of electrons from the simulations increases by 175%, 88%, and 90%, while for OH fluence increases by 1330%, 650%, and 885%, respectively for the same perturbations. These increases are much larger percentage-wise than the relative MB decoloration rate constant increases, though following similar trends. The larger increases described in the simulation may be explained by a saturation of reactive species flux at the interface, particularly in peak regions, that can deplete all interfacial MB concentrations. The experimental results demonstrate pseudo-first order kinetics, which would also align with a saturation of reactive species at the interface. In these cases, both the local streamer propagation as well as the total reactive species flux will contribute to the observed MB decoloration rates.

This simulation highlights how the local plasma morphology can lead to significant changes in radical chemistry across the interface. While the total reactive species densities are important, these localized, spatio-temporal plasma changes will alter diffusion into the interface and thus, local contaminant decomposition. In turbulent flow, these local plasma changes would be expected to be present as well, although over nonuniform, complex surface wave structures. These simulations demonstrate there can be a local plasma impact on contaminant mineralization, although it is difficult to determine the relative magnitude of each effect.

4. Conclusion

From experimentally observing and simulating Faraday waves, several observations can be noted. There is confounding influence of many factors that can spatio-temporally modify chemical reactivity and thus decomposition (decoloration) kinetics. While the bulk plasma is not observed to be impacted by the presence of acoustically driven capillary waves of various wavelengths and amplitudes, the local plasma must change due to polarization of the water surface influencing local electric fields. Notably, the plasma did increase the pseudo first order decoloration rates of MB with the perturbations for both positive and negatively directed streamers, as long as the plasma discharge frequency was kept low. It was interesting to see that at high plasma frequencies, the MB decoloration rate was not influenced by the perturbation. This was determined to be due to the EHD forces driving similar wavelength perturbations. For plasma reactor scale up for treatment applications, increasing the discharge frequency could be an easy way to introduce surface perturbations and thus improve mass transport.

The surface area of the plasma–liquid interface also increases by a factor of around 2.5 with the addition of acoustic perturbations. Nonlinear convective forces at the surface of the Faraday waves can drive an effective convective Stokes drift that can provide mixing and hydrodynamic transport in the liquid.

The discharge polarity also had an influence on the decoloration rates, with negative streamers having higher rates. An increase in the decoloration rate was observed for the 200 Hz driving frequency, along with a similar relative increase in emission area. The emission area generally increased with perturbation, which was similarly observed in plasma simulation code *nonPDPSIM*. The code showed local spatio-temporal changes to the discharge propagation and reactive species flux, which could alter transport at the perturbation level. More work is needed to gain insight on the magnitude of each of these effects (hydrodynamic, surface area, SIW propagation), likely with further simulations, as it would be difficult to isolate any given effect listed. This study is important when considering turbulent flow in plasma–liquid reactor systems, as it attempted to recreate relevant perturbation scales in a repeatable fashion, providing insight into the potential effects of fluid surface perturbations on both transport and plasma morphology.

Data availability statement

The data cannot be made publicly available upon publication because no suitable repository exists for hosting data in this field of study. The data that support the findings of this study are available upon reasonable request from the authors.

Acknowledgments

This material is based upon work supported by the National Science Foundation (NSF) Graduate Research Fellowship under Grant No. DGE-1841052, NSF ECLIPSE Award No. 2206039, and the Anthropocene Institute. We also thank Mark Kushner for the use of his code, *nonPDPSIM*.

ORCID iDs

R Z Walker https://orcid.org/0000-0003-1456-1610
S J Doyle https://orcid.org/0000-0002-8741-1018
J E Foster https://orcid.org/0000-0001-8369-1828

References

[1] Lindsay A, Anderson C, Slikboer E, Shannon S and Graves D 2015 Momentum, heat and neutral mass transport in convective atmospheric pressure plasma-liquid systems and implications for aqueous targets *J. Phys. D: Appl. Phys.* **48** 424007
[2] Lai J, Petrov V and Foster J E 2018 Understanding plasma–liquid interface instabilities using particle image velocimetry and shadowgraphy imaging methods *IEEE Trans. Plasma Sci.* **46** 875–81
[3] Stratton G R, Bellona C L, Dai F, Holsen T M and Mededovic Thagard S 2015 Plasma-based water treatment: conception and application of a new general principle for reactor design *Chem. Eng. J.* **273** 543–50
[4] Mededovic Thagard S, Stratton G R, Vasilev M, Conlon P and Bohl D 2018 An experimental investigation of the liquid flow induced by a pulsed electrical discharge plasma *Plasma Chem. Plasma Process.* **38** 719–41
[5] Chanson H 2009 Turbulent air–water flows in hydraulic structures: dynamic similarity and scale effects *Environ. Fluid Mech.* **9** 125–42
[6] Aranson I S, Rabinovich M I and Sh Tsimring L 1990 Anomalous diffusion of particles in regular fields *Phys. Lett.* A **151** 523–8
[7] Walker R Z and Foster J E 2023 Understanding the influence of fluid flow regime on plasma morphology and dose delivery at the plasma–liquid interface *J. Appl. Phys.* **133** 093301
[8] Faraday M 1831 XVII. on a peculiar class of acoustical figures; and on certain forms assumed by groups of particles upon vibrating elastic surfaces *Phil. Trans. R. Soc. 121* 299–340
[9] Yuan S, Zhang Y and Gao Y 2022 Faraday instability of a liquid layer in ultrasonic atomization *Phys. Rev. Fluids* **7** 033902
[10] Miles J and Henderson D 1990 Parametrically forced surface waves *Annu. Rev. Fluid Mech.* **22** 143–65
[11] Tokugawa N, Umeki M and Kambe T 1995 Statistical analysis of particle drifts on faraday waves *Fluid Dyn. Res.* **16** 43–55
[12] Ramshankar R and Gollub J P 1991 Transport by capillary waves. part II: Scalar dispersion and structure of the concentration field *Phys. Fluids A* **3** 1344–50
[13] Saylor J R and Handler R A 1997 Gas transport across an air/water interface populated with capillary waves *Phys. Fluids* **9** 2529–41
[14] Nikolaevich Kolmogorov A 1941 Equations of turbulent motion in an incompressible fluid *Dokl. Akad. Nauk SSSR* **30** 299–303
[15] Gucker S M N 2015 Plasma discharges in gas bubbles in liquid water: breakdown mechanisms and resultant chemistry *PhD Thesis* University of Michigan
[16] Fellouah H, Ball C G and Pollard A 2009 Reynolds number effects within the development region of a turbulent round free jet *Int. J. Heat Mass Transfer* **52** 3943–54
[17] Durbin P 2001 Turbulent flows. by S B pope. cambridge university press, 2000. 771 pp. ISBN 0 521 59886 9.£29.95 or 130.00 (hardback) *J. Fluid Mech.* **427** 410–1
[18] Norberg S A, Johnsen E and Kushner M J 2015 Formation of reactive oxygen and nitrogen species by repetitive negatively pulsed helium atmospheric pressure plasma jets propagating into humid air *Plasma Sources Sci. Technol.* **24** 035026
[19] Paris P, Aints M, Valk F, Plank T, Haljaste A, Kozlov K V and Wagner H E 2005 Intensity ratio of spectral bands of nitrogen as a measure of electric field strength in plasmas *J. Phys. D: Appl. Phys.* **38** 3894
[20] Bruggeman P J, Kushner M J, Locke B R, Gardeniers J G E, Graham W G, Graves D B, Hofman-Caris R C H M, Maric D, Reid J P and Ceriani E *et al* 2016 Plasma–liquid interactions: a review and roadmap *Plasma Sources Sci. Technol.* **25** 053002
[21] Yu Nikiforov A, Ch Leys M A G and Walsh J L 2015 Electron density measurement in atmospheric pressure plasma jets: stark broadening of hydrogenated and non-hydrogenated lines *Plasma Sources Sci. Technol.* **24** 034001
[22] Voráč J, Synek P, Potočňáková L, Hnilica J and Kudrle V 2017 Batch processing of overlapping molecular spectra as a tool for spatio-temporal diagnostics of power modulated microwave plasma jet *Plasma Sources Sci. Technol.* **26** 025010
[23] Akishev Y, Aponin G, Balakirev A, Grushin M, Karalnik V, Petryakov A and Trushkin N 2011 Memory'and sustention of microdischarges in a steady-state DBD: volume plasma or surface charge? *Plasma Sources Sci. Technol.* **20** 024005
[24] Lai J and Foster J E 2019 Experimental observation of interfacial oscillations and self-organization derived from streamer-driven mechanical perturbation of a gas–liquid boundary *Plasma Sources Sci. Technol.* **28** 125003
[25] Robinson J A and Bergougnou M A 2002 GS Peter castle and ion i inculet. a nonlinear model of ac-field-induced parametric waves on a water surface *IEEE Trans. Ind. Appl.* **38** 379–88
[26] Célestin S, Allegraud K, Canes-Boussard G, Leick N, Guaitella O and Rousseau A 2008 Patterns of plasma filaments propagating on a dielectric surface *IEEE Trans. Plasma Sci.* **36** 1326–7
[27] Levko D, Arslanbekov R R and Kolobov V I 2020 Multi-scale dynamics of atmospheric-pressure discharges ignited over liquid electrodes *J. Appl. Phys.* **127** 043301
[28] Vasilev M, Conlon P, Bohl D and Mededovic Thagard S 2022 The effect of discharge frequency of a gas–liquid plasma reactor on bulk liquid transport and removal of organic contaminants *Plasma Chem. Plasma Process.* **42** 759–83
[29] Gibby C W and Addison C C 1936 283. adsorption at the interface between two fluids. Part II. The adsorption of five dyestuffs at a paraffin–water and at an air–water interface *J. Chem. Soc.* **1936** 1306–13
[30] Mededovic Thagard S, Takashima K and Mizuno A 2009 Chemistry of the positive and negative electrical discharges formed in liquid water and above a gas–liquid surface *Plasma Chem. Plasma Process.* **29** 455–73
[31] Mansoob Khan M, Lee J and Hwan Cho M 2014 Au@TiO_2 nanocomposites for the catalytic degradation of methyl orange and methylene blue: an electron relay effect *J. Ind. Eng. Chem.* **20** 1584–90
[32] Hamdan A, Ridani D A, Diamond J and Daghrir R 2020 Pulsed nanosecond air discharge in contact with water: influence of voltage polarity, amplitude, pulse width and gap distance *J. Phys. D: Appl. Phys.* **53** 355202

[33] Moreau E, Audier P and Benard N 2018 Ionic wind produced by positive and negative corona discharges in air *J. Electrost.* **93** 85–96
[34] van den Bremer T S and Breivik Øyvind 2018 Stokes drift *Phil. Trans. R. Soc. A* **376** 20170104
[35] Francois N, Xia H, Punzmann H, Ramsden S and Shats M 2014 Three-dimensional fluid motion in faraday waves: Creation of vorticity and generation of two-dimensional turbulence *Phys. Rev. X* **4** 021021
[36] Mesquita O N, Kane S and Gollub J P 1992 Transport by capillary waves: Fluctuating stokes drift *Phys. Rev. A* **45** 3700
[37] Shats M, Francois N, Xia H and Punzmann H 2014 Turbulence driven by faraday surface waves *Int. J. Modern Physics: Conf. Series* vol 34 (World Scientific) p 1460379
[38] Vasilev M, Suiter J, Bohl D and Mededovic Thagard S 2023 Caffeine degradation in a plasma-liquid reactor with the lateral liquid flow: Elucidating the effects of mass transport on contaminant removal *Chem. Eng. J.* **473** 144833
[39] Leaist D G 1988 The effects of aggregation, counterion binding and added nacl on diffusion of aqueous methylene blue *Can. J. Chem.* **66** 2452–7
[40] Hamdan A, Diamond J and Herrmann A 2021 Dynamics of a pulsed negative nanosecond discharge on water surface and comparison with the positive discharge *J. Phys. Commun.* **5** 035005
[41] Konina K, Raskar S, Adamovich I V and Kushner M J 2024 Atmospheric pressure plasmas interacting with wet and dry microchannels: reverse surface ionization waves *Plasma Sources Sci. Technol.* **33** 015002